Available online at www.eccomasproceedia.org
Eccomas Proceedia COMPDYN (2017) 1656-1666

ECCOMAS
Proceedia

COMPDYN 2017
6th ECCOMAS Thematic Conference on
Computational Methods in Structural Dynamics and Earthquake Engineering
M. Papadrakakis, M. Fragiadakis (eds.)
Rhodes Island, Greece, 15–17 June 2017

A MODEL FOR NON-LINEAR DYNAMIC ANALYSIS OF SUB-STANDARD REINFORCED CONCRETE MEMBERS

Dimitrios K. Zimos[1], Panagiotis E. Mergos[1], and Andreas J. Kappos[1]

[1] City, University of London
Northampton Square, London EC1V 0HB
e-mail: { Dimitrios.zimos.1, Panagiotis.Mergos.1, Andreas.Kappos.1 }@city.ac.uk

Keywords: Earthquake Engineering, Reinforced Concrete, Hysteretic Behaviour, Post-peak Response, Shear Failure, Bearing Capacity.

Abstract. *Reinforced concrete (R/C) buildings designed according to older seismic codes represent a large part of the existing building stock; hence, it is important to be able to accurately assess their response to seismic actions. These substandard R/C buildings may contain structural elements that are prone to shear failure subsequent, or even prior, to yielding of their longitudinal reinforcement. This can potentially lead to loss of axial load resistance of vertical elements and initiate vertical progressive collapse of the building.*

In the present study, a model is put forward, which is able to capture the hysteretic behaviour of shear critical R/C elements up to the onset of axial failure. The model is able to account for gradual spread of inelasticity and shear-flexure interaction in the locations of the plastic hinges prior to the onset of shear failure as well as localisation of shear strains after the onset of shear failure; the latter constitutes a major advancement in the existing literature.

The model is used to predict the behaviour of a cyclically loaded double-curvature specimen failing axially after shear failure and flexural yielding. The comparison of the analytical with the experimental results shows a very good agreement, both in terms of total response and of shear response.

Peer-review under responsibility of the organizing committee of COMPDYN 2017.
doi: 10.7712/120117.5520.17845

1 INTRODUCTION

R/C buildings designed according to older seismic codes (or even without adhering to any code) represent a large part of the existing building stock worldwide. Thus, it is important to be able to accurately and efficiently assess their response to earthquake-induced actions, in order to evaluate their vulnerability. Transverse reinforcement in their structural elements is typically inadequate - widely spaced and/or poorly anchored - rendering them vulnerable to shear failure subsequent, or even prior, to yielding of their longitudinal reinforcement. This can eventually lead to loss of axial resistance of vertical elements, through disintegration of the poorly confined concrete core and the consequent axial resistance decrease [1], and initiate vertical progressive collapse of a building. This collapse type has been shown through post-earthquake reconnaissance to be the most common reason of R/C frame building collapse [2].

The total displacement of an R/C member under lateral loading consists of three components, i.e. flexural, anchorage slip and shear displacements [3]. The former can be captured quite accurately by the available finite element models, providing an accurate prediction of the response of a well-designed element conforming to current seismic codes. Nevertheless, the other two components readily become significant in sub-standard members and have to be accounted for in order to obtain an accurate response prediction.

It has been observed experimentally that in regions of inelastic flexural deformations, shear strength degradation is triggered even if no shear yielding has taken place [4],[5] and that even if shear demand does not increase, shear deformations may increase considerably [3]. This impacts the response of flexure-shear critical members that fail in shear after experiencing flexural yielding. Several models have been developed to predict the degradation of shear strength with ductility demand in such members. Amongst them, some well-known ones are the model by Priestley *et al*. [6] and a revised version of it for circular columns [7], Sezen & Moehle's model [8], and a more recent one, based on statistical analysis of a large number of flexure-shear critical column specimens, by Biskinis *et al*. [9].

Advanced shear response models like the Modified Compression Field Theory (e.g. [10]) or the softened truss and membrane models by Hsu et al. (e.g. [11], [12]) are based on structural mechanics and have proven to be rather accurate, but they are limited to pre-peak shear behaviour. More recently, the Axial-Shear-Flexure Interaction approach was proposed [13], considering post-peak shear response. Nonetheless, these approaches require excessive computational demand and do not capture the hysteretic response of R/C elements, thus do not lend themselves to use in seismic analysis of complex R/C structures.

Furthermore, there have been several *macro-models*, especially in the last two decades, aiming at modelling the cyclic lateral behaviour of shear-deficient R/C elements considering shear-flexure interaction effects (e.g. [3], [14]–[18]). Some of them also extend into the post-peak domain of the response, thus being capable of predicting the onset of axial failure of an element, which is critical in assessing the behaviour of an existing structure, especially when it comes to predicting the initiation and cascade of progressive collapse. Most of these models are based on inter-storey drift ratios, despite the fact that localised drift ratios at the shear-damaged regions might be more appropriate, since shear deformations tend to concentrate there after the onset of shear failure (e.g. [19], [20]); this effect, hereafter called *shear failure localisation*, corresponds essentially to the relative rigid body displacement between the discrete upper and lower bodies of a column along the diagonal shear failure plane.

A model for the full-range hysteretic shear response of substandard elements is presented in this study accounting for the afore-described shear failure localisation effect. Being based on shear deformations instead of an inter-storey shear displacement, it can more objectively

account for the interaction of inelastic flexural and shear deformations at a local level, including the gradual decrease of an element's shear resistance, and more reliably predict the location and extent of the shear failure zone, without relying on assumptions about the bending moment distribution. The shear model is incorporated in the computationally efficient phenomenological flexibility-based, spread-inelasticity beam-column model by Mergos & Kappos [3], with a view to accurately capturing the hysteretic response of shear-deficient R/C elements and structures up to the onset of axial failure. In the following, the proposed model is presented in detail and its predictive capabilities are verified against experimental results, not only in terms of total displacement, but, more critically, also in terms of the shear displacement component per se.

2 ANALYTICAL MODEL DESCRIPTION

2.1 Beam-column model

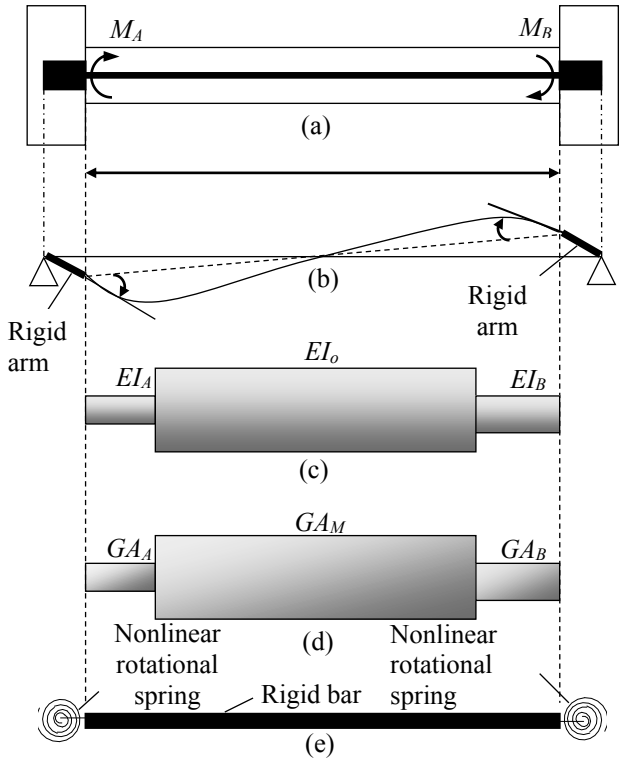

Figure 1: Finite element model: (a) geometry of R/C member; (b) beam–column finite element with rigid offsets; (c) flexural sub-element; (d) shear sub-element; (e) anchorage slip sub-element. [3]

The beam-column model is a phenomenological flexibility-based finite element model [3] with three sub-elements connected in series, accounting for flexural, shear and anchorage slip deformations, respectively (Figure 1). The element flexibility matrix F is produced by the summation of the flexibility matrices of the flexural F^{fl}, shear F^{sh} and anchorage-slip F^{sl} sub-elements and its inversion results in the element stiffness matrix K:

$$K = F^{-1} = (F^{fl} + F^{sh} + F^{sl})^{-1} \tag{1}$$

The flexural sub-element is divided into an elastic intermediate region and two end regions, where flexural yielding takes place. A spread inelasticity model is employed to follow the gradual inward penetration of yielding from the ends of each sub-element. This model

distinguishes between loading and unloading or reloading states, leading respectively to different stiffness distribution in the end-regions [21]. The flexural sub-element's (Figure 1c) primary M-φ curve is based on standard flexural analysis and appropriate bilinearization of the resulting curve. The hysteretic rules applied are described in detail in [3].

Prior to the onset of shear failure, the shear sub-element has a flexibility distribution similar to the flexural sub-element (Figure 1d). Shear-flexure interaction is considered in its inelastic end regions, the lengths of which are set equal to the lengths of the respective regions of the flexural sub-element. A more detailed description of the shear sub-element with emphasis on the response after the onset of shear failure is provided in the following sections.

The anchorage slip sub-element (Figure 1e) consists of two concentrated springs at the ends of the element, representing the rotations arising at the interfaces of adjacent R/C members, due to slippage of the reinforcement anchorage in the joints. The derivation of the primary M-θ_{slip} curve, as well as the hysteretic rules used, are presented in detail elsewhere [3].

2.2 Shear sub-model description

The shear sub-element's (Figure 1d) primary V-γ curve is originally defined disregarding interaction with flexure and is used for elements that have not yielded in flexure as well as for the region outside the plastic hinges for members that have yielded (Figure 2). This curve is defined by the shear cracking point (nominal tensile principal stress exceeding the tensile concrete strength), the onset of yielding of the transverse reinforcement, where the maximum shear strength is attained, and a plateau, where shear strains increase with constant force up to the onset of initiation of lateral strength degradation, i.e. the onset of shear failure.

Subsequently, a descending branch [22] is followed up to the onset of axial failure with a slope $S_{pp} \times V_{max}$ (Figure 2). The definition of axial failure is both deformation-based and force-based. A column is considered to have failed axially (i.e. lost its bearing capacity) if the shear deformation limit corresponding to the onset of axial failure $\gamma_{sh,f} + \gamma_{t,pp}$ has been reached (Figure 2), namely the shear distortion at the onset of shear failure plus the total post-peak shear distortion [22]. However, if shear strength degrades to zero prior to the deformation limit being reached, the point with zero shear strength is considered as the onset of axial failure, i.e. shear strength is not allowed to assume negative values.

The V-γ curve is subsequently altered in plastic hinge regions, accounting for shear-flexure interaction. This is based on flexural ductility and the ensuing degradation of the 'concrete contribution' to shear strength, resulting in increase of the truss contribution. The parts of the backbone curve between the shear strength corresponding to flexural yielding (V_y in Figure 2) and the onset of shear failure are affected. More details are given elsewhere [3].

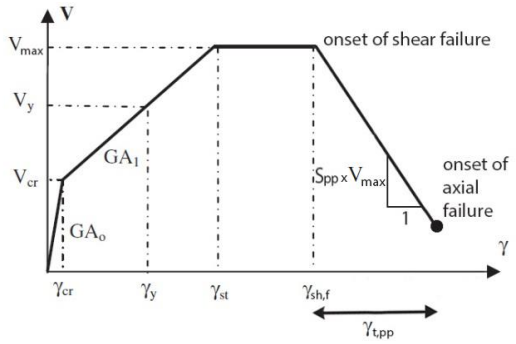

Figure 2: V-γ primary curve of the proposed model without shear-flexure interaction. [22]

After the onset of shear failure, the basic assumption adopted in this study is that flexural and slip-induced deformations do not increase further than their values at onset of failure, i.e. all post-peak deformations occur in the shear sub-element. This assumption has been adopted in similar models (e.g. [23], [24]) and is supported by experimental evidence (e.g. [25]).

Furthermore, it has been previously established based on experimental observations (e.g. [19], [20]) that deformations after the onset of shear failure tend to concentrate at a specific member region, the "*critical length*" defined by the diagonal failure plane; this length is illustratively shown in Figure 3 with distorted scale for the displacements, where the clear length of the column, L_{cl}, and the critical length, L_{cr} are shown. The localisation of post-peak shear strains is herein called "shear failure localisation" [22]; in essence, it mainly represents the relative rigid body displacement between the discrete upper and lower bodies of the column along the shear crack (Figure 3).

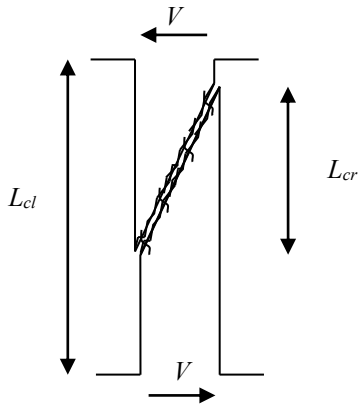

Figure 3: Illustrative sketch of the critical length in a shear-damaged column.

The hysteretic rules adopted in the shear sub-model are based on those of Ozcebe & Saatcioglu [4], with several improvements. Pinching, unloading and reloading stiffness deterioration, as well as post-peak cyclic strength degradation, are accounted for. Shear strength degradation mirroring is also taken into account. This effectively means that once a certain amount of strength is lost in one loading direction, a higher strength cannot be reached in the other. This assumption has been adopted by other similar models (e.g. [18]) and is supported by experimental evidence (e.g. [19], [1]).

2.3 Shear sub-model implementation

The proposed finite element model has been implemented in IDARC2D [26]. The prescribed post-peak V - γ descending branch (eq. 4-12) is followed subsequent to the onset of shear failure (defined as described in [3]). This is realised by a commensurate drop in the current force, the yield strength, as well as the entire post-yield branch of the shear backbone, as shown schematically in Figure 4. This way, the stiffness is always positive, hence no instability occurs anywhere in the algorithm. The amount of strength deterioration at each solution step equals the exceedance of strength at the same step with respect to the strength of the target post-peak branch with the same shear strain.

An illustrative hysteretic response of a specimen - without *cyclic* strength degradation, for clarity - is shown in Figure 5, wherein the application of shear strength degradation mirroring is demonstrated. The descent starts from the onset of shear failure with V_{max} on the positive side, followed by $\Delta V_{1,pos}$ *in-cycle* degradation. The vertex point ordinate in the negative direction becomes - (V_{max} - $\Delta V_{1,pos}$). Similarly, the in-cycle degradation on the negative side

($\Delta V_{1,neg}$) is subtracted from the positive vertex point force upon reloading on the positive side for the first time, and so forth.

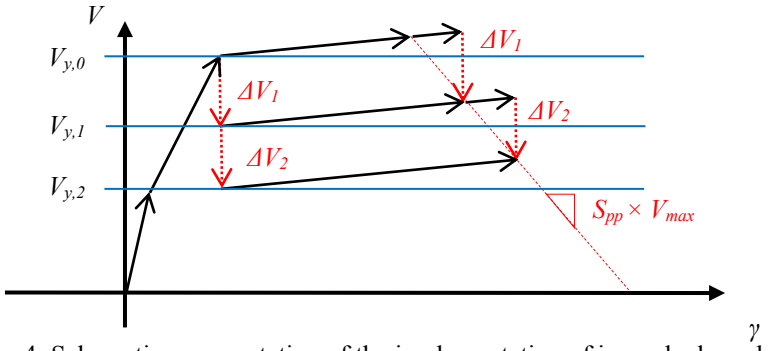

Figure 4: Schematic representation of the implementation of in-cycle degradation.

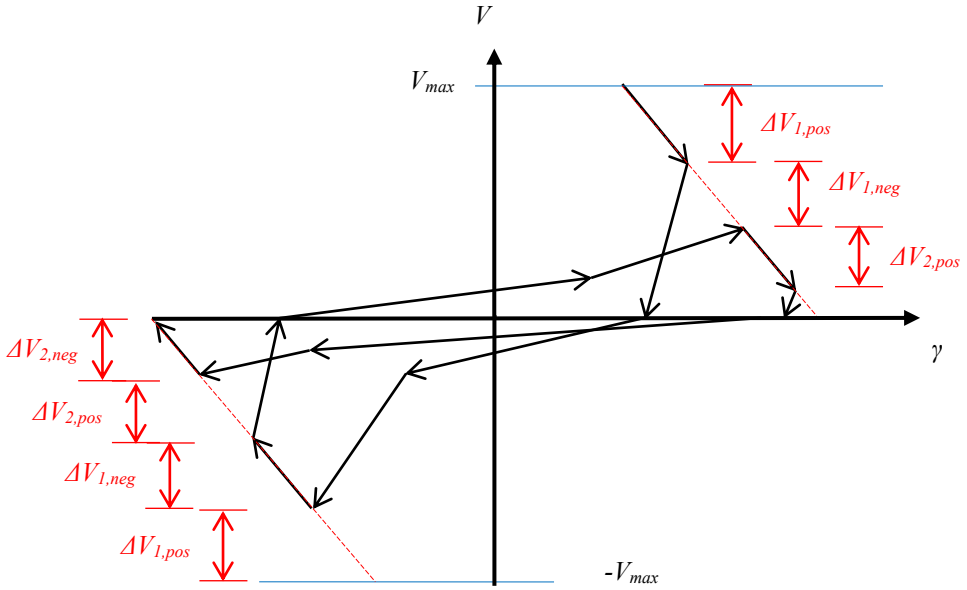

Figure 5: Illustrative hysteresis of a specimen from onset of shear failure up to onset of axial failure.

As discussed previously, prior to shear failure, the shear sub-element is subdivided into two end regions representing the locations where flexural yielding takes place and an intermediate region for the rest of the member (Figure 1d). After the onset of shear failure, localisation of shear strains is realised by setting the length of the region, where shear failure is detected, equal to the shear critical length (Figure 6). Following this approach, the location and extent of the shear failure zone is predicted accurately by considering the interaction of inelastic flexural and shear deformations at a local level. Therefore, the actual phenomenon is more realistically depicted. In addition, the response after the onset of shear failure is predicted in an accurate and objective manner that is not relying on assumptions regarding bending moment distribution of R/C members. This is clearly not the case with models using total shear displacement components, instead of local deformation quantities.

In line with experimental evidence, the shear failure plane is always unique, therefore the model invariably results in only one of the three segments failing. In Figure 6, the transition from pre-peak to post-peak for the generic cases of a flexure-shear and a shear critical specimen can be seen as well as the corresponding shear flexibility coefficients; α_{As} and α_{Bs} are defined as the shear-flexural yield penetration coefficients, which monitor the penetration

of yield from the end A or B, respectively, towards the middle of the element; GA_A, GA_B and GA_M are the corresponding stiffness of the end A, end B and middle segment sections of the element.

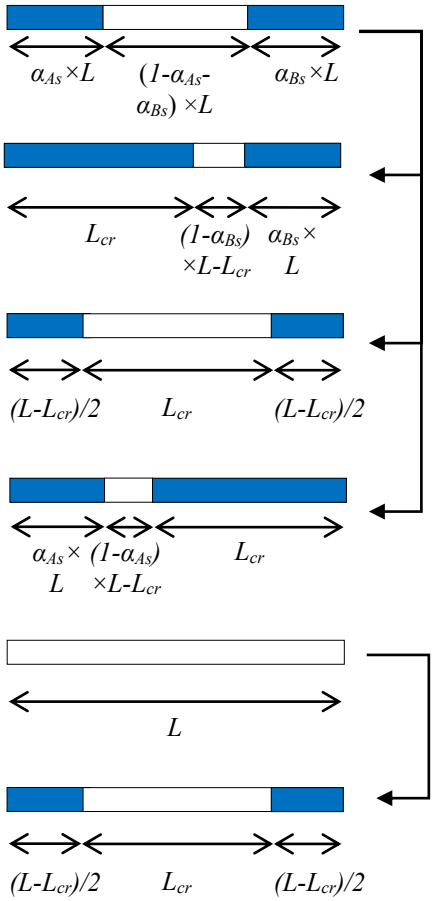

$$f_{ij}^{sh} = \frac{a_{As}}{GA_A \times L} + \frac{1 - a_{As} - a_{Bs}}{GA_M \times L} + \frac{a_{Bs}}{GA_B \times L} \quad (2)$$

$$f_{ij}^{sh} = \frac{L_{cr}}{GA_A \times L^2} + \frac{1 - L_{cr}/L - a_{Bs}}{GA_M \times L} + \frac{a_{Bs}}{GA_B \times L} \quad (3)$$

$$f_{ij}^{sh} = \frac{1 - L_{cr}/L}{2 \times GA_A \times L} + \frac{L_{cr}}{GA_M \times L^2} + \frac{1 - L_{cr}/L}{2 \times GA_B \times L} \quad (4)$$

$$f_{ij}^{sh} = \frac{a_{As}}{GA_A \times L} + \frac{1 - a_{As} - L_{cr}/L}{GA_M \times L} + \frac{L_{cr}}{GA_B \times L^2} \quad (5)$$

$$f_{ij}^{sh} = \frac{1}{GA_M \times L} \quad (6)$$

$$f_{ij}^{sh} = \frac{1 - L_{cr}/L}{2 \times GA_A \times L} + \frac{L_{cr}}{GA_M \times L^2} + \frac{1 - L_{cr}/L}{2 \times GA_B \times L} \quad (7)$$

Figure 6: Spread inelasticity distributions and respective shear flexibility coefficients for a flexure-shear critical specimen (top) with failure at end A (Eq. 3), failure at end B (Eq. 5) or failure in the middle (Eq. 4) for a given pre-peak distribution (Eq. 2) with i,j = A, B. Similarly, for a shear critical specimen (bottom) with failure (Eq. 7) from the pre-peak distribution (Eq. 6).

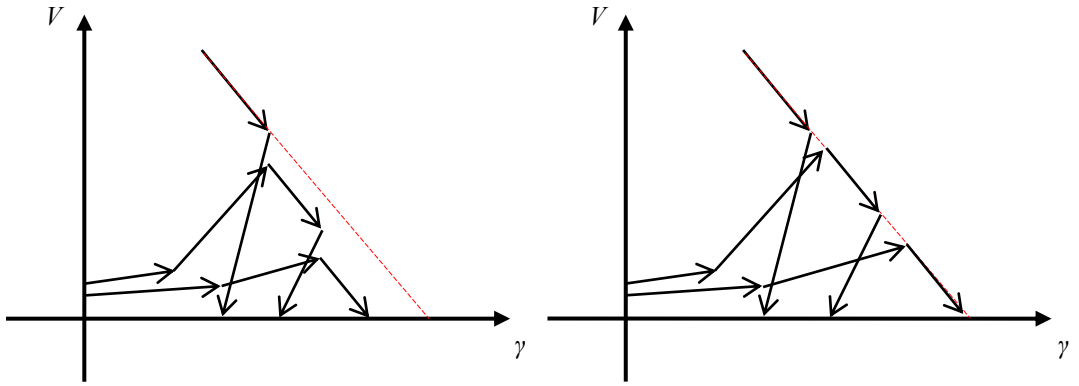

Figure 7: Schematic representation of the descending branch offset due to cyclic degradation (left) and the response with compensation for this offset (right).

Cyclic strength degradation is taken into consideration in the post-peak domain using the Ozcebe & Saatcioglu [4] rules. However, that creates a permanent loss of strength, which distorts the produced descending branch and leads to slightly premature onset of axial failure in the case of shear strength reaching zero (Figure 7a). A compensation algorithm has been employed, in order to avoid this shift; instead of aiming at the previous vertex deformation with a reduced vertex strength, as originally proposed [4], the target is the intersection of that line and the descending branch; hence, the resulting behaviour is as intended (Figure 7b). Besides strength degradation, pinching as well as unloading and reloading stiffness deterioration are accounted for using the same set of rules as described in [4].

3 ANALYTICAL MODEL VERIFICATION

Sezen & Moehle [1] tested four double-curvature columns with different axial loads under quasi-static cyclic loading. They were lightly reinforced, representative of old-type construction, designed to yield in flexure and subsequently fail in shear. The column Specimen-1, tested under an axial load of 667 kN, is herein selected for verification of the proposed analytical model. Its clear height was 2946 mm, with a square cross-section of 457×457 (mm) and a longitudinal reinforcement ratio of 2.5%. The transverse reinforcement comprised rectangular and diamond-shaped ties every 305 mm, with 90^o anchorage hooks. The concrete compressive strength was 21 MPa and the longitudinal and transverse reinforcement yield strengths were 434 MPa and 476 MPa, respectively. The empirical relations proposed in [22] were used to model the descending branch slope, the critical length and the deformation at the onset of axial failure.

The proposed model seems to be capturing the pre- and post-peak hysteretic response fairly well (Figure 8a). It matches very well the overall behaviour, with unloading and reloading stiffnesses of the analysis representing very well the average stiffnesses observed experimentally, and capturing very well the very high strength degradation at the displacement level of ±42 mm. Of course, there is certain deviation at given points; especially on the negative direction. The maximum strength is shown to be very accurate, with negligible overestimation. There is some underestimation of the expected displacement at the onset of axial failure, being however close to the experimental value. The onset of axial failure was predicted at the first of the three cycles of the ±55 mm displacement level. This is due to the fact that the descending branch was calculated slightly steeper than its experimental value. Even so, the predicted energy dissipation, which is a key characteristic of the hysteretic response, is overestimated only by approximately 10% compared to the actual energy dissipated by the member during the cyclic test.

The shear displacement component is captured very well both in the pre- and post-peak domain (Figure 8b), given the challenge of predicting individual (i.e. shear) displacement components instead of the total response and the inherent uncertainty of experimental measurements. There is a negligible underestimation of shear deformations before the peak, but upon shear failure the experimental shear displacement increases considerably in the positive direction, a tendency which the model captures sufficiently. Subsequently, there is a slight underestimation of shear displacements on the negative side of the post-peak cycle, nonetheless following the general trend. Not all shear response history is provided by the researchers that carried out the test, possibly due to failure of the recording instrument, therefore only one full experimental post-peak cycle is presented in Figure 8. Nevertheless, even the first post-peak cycle is enough to demonstrate that although shear displacements are only a small fraction of the total in the pre-peak domain, as soon as the peak is reached they immediately take up a very big portion of it. Figure 8c shows the analysis of the components of the lateral displacement of the element; it is observed that shear displacements are very low

in the first stages of the response, increasing significantly after the element yields, due to shear-flexure interaction at the ends of the member. Furthermore, they increase drastically after the onset of shear failure, as all the post-peak displacements are attributed to the shear sub-element; the flexural and bond-slip displacements, on the other hand, do not exceed their maximum pre-peak values at any point in the post-peak domain.

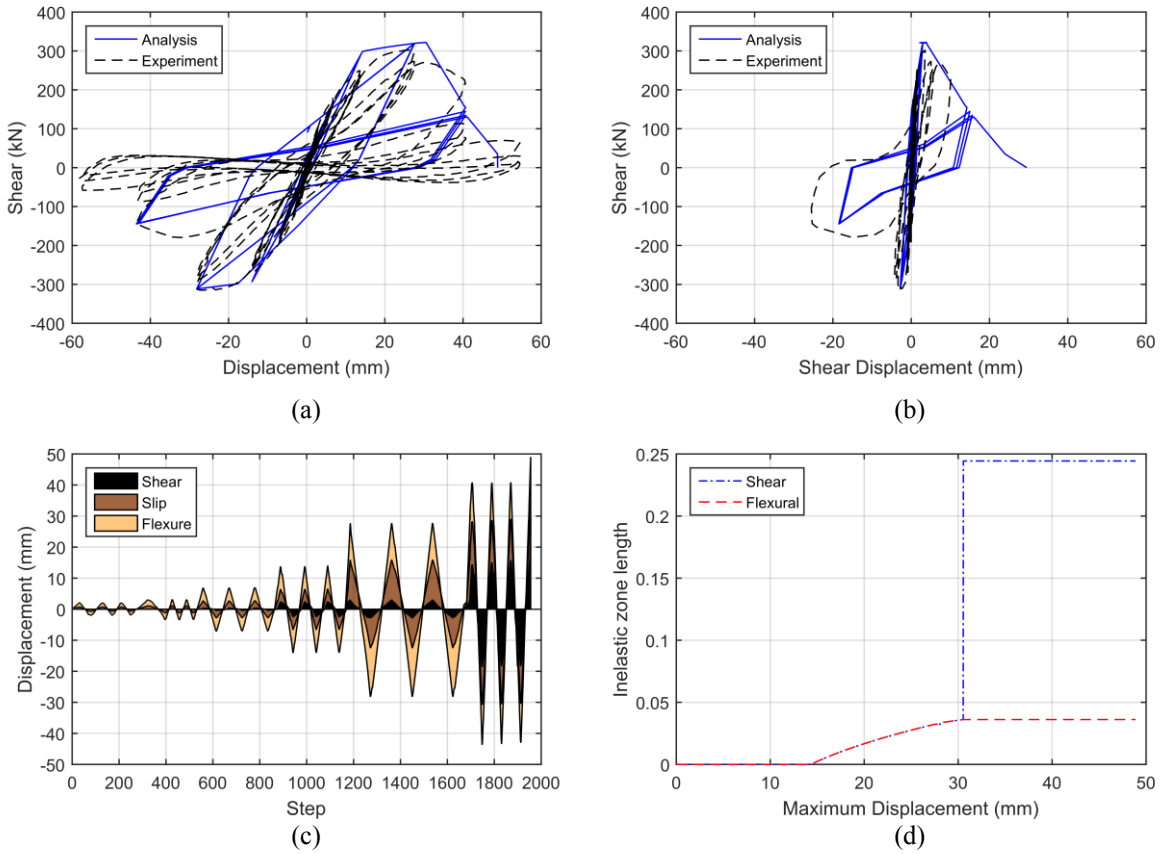

Figure 8: Sezen & Moehle's [1] Specimen-1: Comparison between predicted response by the proposed model and experimental one in terms of shear force against lateral displacement (a), (part of) shear force against shear displacement (b); analysis of the element's lateral displacement components (c) and flexural and shear inelastic zone lengths as a percentage of the total member length at each displacement level of the analysis (d).

Figure 8d demonstrates the spread of inelasticity during the analysis for the flexural and shear sub-elements. After the onset of flexural yielding, the inelastic end zones of both the flexural and shear sub-element increase gradually following the moment increase at the member ends. Nonetheless, as soon as the onset of shear failure is reached just after 30 mm maximum displacement, the length of the inelastic zone of the shear sub-element instantly assumes a value corresponding to the shear critical length and maintains it for the rest of the analysis. At the same time, the length of the inelastic zone of the flexural sub-element remains equal to the maximum value reached at the onset of shear failure.

4 CONCLUSIONS

The development of a shear model for the full-range hysteretic response of substandard R/C elements was presented herein. It is integrated in a phenomenological flexibility-based spread-inelasticity model that accounts for shear-flexure interaction, with a view to accurately capturing the response of shear-deficient R/C elements and structures. Being based on (local) shear distortions instead of an inter-storey shear displacement, it can account in an unbiased

way for the interaction of inelastic flexural and shear deformations at a local level, including the gradual decrease of an element's shear resistance, and more reliably predict the location and extent of the shear failure zone, without relying on assumptions regarding the bending moment distribution. It is the first shear model directly accounting for the localisation of shear strains, after the onset of shear failure, in a critical length defined by a diagonal failure plane, namely shear failure localisation.

The model has been verified here against a double-curvature flexure-shear critical column quasi-static test and was found to provide a very good estimation of the overall response. More importantly, it was shown to fare satisfactorily not only in terms of total lateral displacement, but also in terms of shear displacement.

5 ACKNOWLEDGEMENTS

This research study was conducted as part of the doctoral degree of the first author funded by City, University of London and the A. G. Leventis Foundation.

REFERENCES

[1] H. Sezen, J. Moehle, Seismic tests of concrete columns with light transverse reinforcement. *ACI Structural Journal*, **103**, 842–849, 2006.

[2] W. M. Ghannoum, J. P. Moehle, Y. Bozorgnia, Analytical collapse study of lightly confined reinforced concrete frames subjected to Northridge earthquake ground motions. *Journal of Earthquake Engineering*, **12**, 1105–1119, 2008.

[3] P. E. Mergos, A. J. Kappos, A gradual spread inelasticity model for R/C beam–columns, accounting for flexure, shear and anchorage slip. *Engineering Structures*, **44**, 94–106, 2012.

[4] G. Ozcebe, M. Saatcioglu, Hysteretic shear model for reinforced concrete members. *Journal of structural engineering*, **115**, 132–148, 1989.

[5] J.-Y. Lee, F. Watanabe, Predicting the longitudinal axial strain in the plastic hinge regions of reinforced concrete beams subjected to reversed cyclic loading. *Engineering Structures*, **25**, 927–939, 2003.

[6] M. Priestley, R. Verma, Y. Xiao, Seismic shear strength of reinforced concrete columns. *Journal of structural engineering*, **120**, 2310–2329, 1994.

[7] M. Kowalsky, M. Priestley, Improved analytical model for shear strength of circular reinforced concrete columns in seismic regions. *ACI Structural Journal*, **97**, 388–396, 2000.

[8] H. Sezen, J. Moehle, Shear strength model for lightly reinforced concrete columns. *Journal of Structural Engineering*, **130**, 1692–1703, 2004.

[9] D. Biskinis, G. Roupakias, M. Fardis, Degradation of shear strength of reinforced concrete members with inelastic cyclic displacements. *ACI Structural Journal*, **101**, 773–783, 2004.

[10] F. Vecchio, M. Collins, The modified compression-field theory for reinforced concrete elements subjected to shear. *ACI Journal Proceedings*, **83**, 219–231, 1986.

[11] T. T. C. Hsu, Softened truss model theory for shear and torsion. *Structural Journal*, **85**, 1988.

[12] T. T. C. Hsu, R. R. H. Zhu, Softened membrane model for reinforced concrete elements in shear. *ACI Structural Journal*, **99**, 460 – 469, 2002.

[13] H. Mostafaei, T. Kabeyasawa, Axial-shear-flexure interaction approach for reinforced concrete columns. *ACI Structural Journal*, **104**, 218–226, 2007.

[14] D. Lee, A. Elnashai, Inelastic seismic analysis of RC bridge piers including flexure-shear-axial interaction. *Structural Engineering and Mechanics*, **13**, 241–260, 2002.

[15] J. Pincheira, F. Dotiwala, J. D'Souza, Seismic analysis of older reinforced concrete columns. *Earthquake Spectra*, **15**, 245–272, 1999.

[16] H. Sezen, T. Chowdhury, Hysteretic model for reinforced concrete columns including the effect of shear and axial load failure. *Journal of Structural Engineering*, **135**, 139–146, 2009.

[17] M. Baradaran-Shoraka, K. J. Elwood, Mechanical model for non-ductile reinforced concrete columns. *Journal of Earthquake Engineering*, **17**, 937–957, 2013.

[18] M. R. LeBorgne, W. M. Ghannoum, Analytical Element for Simulating Lateral-Strength Degradation in Reinforced Concrete Columns and Other Frame Members. *Journal of Structural Engineering*, **140**, 04014038, 2013.

[19] K. Henkhaus, S. Pujol, J. Ramirez, Axial failure of reinforced concrete columns damaged by shear reversals. *Journal of Structural Engineering*, **139**, 1172–1180, 2013.

[20] K. Elwood, J. Moehle, Axial capacity model for shear-damaged columns. *ACI Structural Journal*, **102**, 578–587, 2005.

[21] D. K. Zimos, P. E. Mergos, A. J. Kappos, Shear hysteresis model for reinforced concrete elements including the post-peak range. in *COMPDYN 2015: 5th ECCOMAS Thematic Conference on Computational Methods in Structural Dynamics and Earthquake Engineering*, Crete Island, Greece, May 25–27, 2015.

[22] P. Mergos, A. Kappos, Analytical study on the influence of distributed beam vertical loading on seismic response of frame structures. *Earthquakes and Structures*, **5**, 239–259, 2013.

[23] H. Sezen, Shear deformation model for reinforced concrete columns. *Structural Engineering and Mechanics*, **28**, 39–52, 2008.

[24] K. Elwood, Modelling failures in existing reinforced concrete columns. *Canadian Journal of Civil Engineering*, **31**, 846–859, 2004.

[25] N. Shirai, B. A. Lejano, H. Adachi, M. Nakanishi, Flexure and shear behavior of high strength reinforced concrete column subjected to high and fluctuating axial load. in *11th World Conference on Earthquake Engineering*, 1996.

[26] A. Reinhorn, H. Roh, M. Sivaselvan, S. K. Kunnath, R. Valles, A. Madan, C. Li, R. Lobo, Y. J. Park, IDARC2D Version 7.0: A Program for the Inelastic Damage Analysis of Structures. Technical Report MCEER-09-0006, 2009.